

Hybrid Laser-arc Welding of 17-4 PH Martensitic Stainless Steel

Wei Liu · Junjie Ma · Mehdi Mazar Atabaki · Raju Pillai ·
Biju Kumar · Unnikrishnan Vasudevan · Harold Sreshta ·
Radovan Kovacevic

Accepted: 30 January 2015 / Published online: 10 February 2015
© Springer New York 2015

Abstract 17-4 PH stainless steel has wide applications in severe working conditions due to its combination of good corrosion resistance and high strength. The weldability of 17-4 PH stainless steel is challenging. In this work, hybrid laser-arc welding was developed to weld 17-4 PH stainless steel. This method was chosen based on its advantages, such as deep weld penetration, less filler materials, and high welding speed. The 17-4 PH stainless steel plates with a thickness of 19 mm were successfully welded in a single pass. During the hybrid welding, the 17-4 PH stainless steel was immensely susceptible to porosity and solidification cracking. The porosity was avoided by using nitrogen as the shielding gas. The nitrogen stabilized the keyhole and inhibited the formation of bubbles during welding. Solidification cracking easily occurred along the weld centerline at the root of the hybrid laser-arc welds. The microstructural evolution and the cracking susceptibility of 17-4 PH stainless steel were investigated to remove these centerline cracks. The results showed that the solidification mode of the material changed due to high cooling rate at the root of the weld. The rapid cooling rate caused the transformation from ferrite to austenite during the solidification stage. The solidification cracking was likely formed as a result of this cracking-susceptible microstructure and a high depth/width ratio that led to a high tensile stress concentration. Furthermore, the solidification cracking was prevented by preheating the base metal. It was found that the preheating slowed the cooling rate at the root of the weld, and the ferrite-to-austenite transformation during the solidification stage was suppressed. Delta ferrite formation was observed in the weld bead as well no solidification cracking occurred by optimizing the preheating temperature.

W. Liu · J. Ma · M. M. Atabaki · R. Kovacevic (✉)
Research Center for Advanced Manufacturing, Southern Methodist University, 3101 Dyer Street, Dallas,
TX 75205, USA
e-mail: kovacevi@lyle.smu.edu

R. Pillai · B. Kumar · U. Vasudevan · H. Sreshta
National Oilwell Varco, Conroe, TX, USA

Keywords Martensitic precipitation-hardened stainless steel · Hybrid laser-arc welding · Porosity · Solidification cracking

Introduction

17-4 PH steel (AISI type 630) is a martensitic precipitation-hardened (PH) stainless steel (SS) that exhibits good corrosion resistant and excellent strength. It has extensive applications in severe service conditions in oil and gas, shipbuilding, chemical, and aerospace industries [1]. Similar to austenitic stainless steels, the high content of chromium determines the good corrosion-resistant property of 17-4 PH SS. The high strength is accomplished by a martensitic microstructure in combination with precipitation hardening. The martensite occurs after solution annealing. When the solution-annealed materials are aged within the temperature range of 450 °C to 510 °C, their maximum strength and hardness are obtained due to the formation of coherent copper-rich precipitates [2]. Reverted austenite and recrystallized ferrite are formed when the materials are overaged at temperatures greater than 580 °C. The plastic phases increase the toughness of 17-4 PH SS and relax its brittle quality [3].

The welding of 17-4 PH SS is much like welding of austenitic stainless steel [4]. It is well suited for the arc welding processes, such as gas tungsten arc welding (GTAW). When welding thin steel plates, the 17-4 PH SS is typically welded in a solution-annealed condition. For thick plates, welding the material in an overaged condition is preferred. In which case, the inherent material restraint and crack susceptibility are reduced [5]. Preheating is normally unnecessary during the arc welding of 17-4 PH SS [6]. However, preheating and a certain temperature between passes are used during the welding of thick plates [4]. Previous studies on the welding of 17-4 PH SS centered on the post-weld heat treatment of the welds. The post-weld heat treatment obtained excellent mechanical and corrosion-resistant properties. Similar to the response of the base material to the heat treatment, a high strength of 17-4 PH SS weld was achieved at an aged condition while the impact toughness of the welds increased at an overaged condition [4]. The corrosion resistance of the 17-4 PH SS welds increased after the post-weld heat treatment [7]. Nowacki [8] reported that a good corrosion resistance was achieved when the aging temperature was higher than 620 °C.

Das et al. [4] welded 12-mm thick 17-4 PH SS by using GTAW in a single bevel groove configuration. The 14 weld passes were performed to fill the weld joint. Bhaduri et al. [9] welded 25-mm thick 17-4 PH SS in a double-V configuration. GTAW was selected to conduct the root pass while the rest of the passes were performed by shielded metal arc welding (SMAW). Welding of 17-4 PH SS by using a high-density power source, such as laser beam, has rarely been reported. With respect to the traditional arc welding, the advantages of laser-aided welding techniques are less heat input and consequently less distortion, higher welding speed, deeper weld penetration, and easier automation. Webster et al. [10] studied the hybrid laser-arc welding of thick steel plates and they reported that up to 25-mm thick high-strength steel plates were successfully welded in a single pass by using a laser of 20 kW in power. Sound welds with good mechanical properties were achieved. In another study, Jokinen and Karhu [11] used 3 kW Nd: YAG laser beam to weld 20-mm thick austenitic stainless steel. Limited by the power level of the selected laser, multipasses were performed.

With respect to the arc welding, the use of filler materials decreased, and less passes were achieved with a narrow weld zone.

In this study, a 10-kW TRUMPF disk laser was used to conduct the hybrid laser-arc welding of the 19-mm thick 17-4 PH SS. The welding procedure was optimized to achieve the full weld penetration in a single pass. The effects of welding parameters on the formation of porosity were investigated. The microstructural evolution and cracking susceptibility of 17-4 PH SS welds were studied to eliminate the solidification cracks along the weld centerline.

Experimental Setup

The 17-4 PH SS plates in an H1150 overaged condition were welded by using hybrid laser-arc welding. Table 1 shows detailed information about the H1150 heat treatment [1]. ER630 with a diameter of 0.9 mm was selected as the filler wire. The chemical compositions of 17-4 PH SS plates and ER630 filler wire are given in Table 2 [7]. The microstructure of the 17-4 PH SS plate is given in Fig. 1. The microstructure consisted of the tempered martensite and the recrystallized alpha ferrite that was formed in the martensite matrix during the overaged treatment [12].

The experimental setup for the hybrid laser-arc welding is shown in Fig. 2a. A TRUMPF TruDisk 10003 laser with a power of 10 kW was used to weld the 17-4 PH coupons. The continuous wave (CW) Yb:YAG diode-pumped disk laser with a wavelength of 1064 nm was connected to a laser welding head through an optical fiber of 300 μm in diameter. The laser welding head was equipped with reflective focusing optics of 300 mm in focal length. The CLOOS gas metal arc (GMA) power source was applied. A 6-axis high-precision KUKA KR 60–3 robot was used to achieve the motion needed during welding. As shown in Fig. 2b, an induction heater was used to preheat the welded joints. Thermocouple was selected to measure the preheating temperature. The designed induction probe was large enough to cover the entire coupon in this research. However, for the larger structures, the designed induction probe would move together with the laser welding head in order to cover larger welds.

Figure 3a shows the schematic diagram of the Y-joint configuration used in this work. Previous work done by the authors [13] investigated the effects of welding parameters on the synergistic effect between laser beam and arc. Based on this work, the geometry parameters, such as offset distance and laser focal position, were determined to achieve the synergistic interaction between laser beam and arc, as shown in Fig. 3b. Table 3 shows the welding parameters used in this study. An abrasive water-jet cutting machine was used to cut the steel plates and to cross-section the weld beads. All coupons were cleaned with methyl alcohol before being etched with a solution (5 g FeCl_3 +25 mL HCl+10 mL H_2O). An optical microscope and a scanning electron

Table 1 Heat treatment conditions for 17-4 PH stainless steel

Condition	Heated to	Time at temperature	Cooling
Solution annealing	1038 °C (1900 °F)	0.5 h	air
H1150 after the solution annealing	621 °C (1150 °F)	4 h	air

Table 2 Chemical compositions of the welded materials and filler wire (%)

	C	Mn	P	S	Si	Cr	Ni	Mo	Cu	Nb+V
17-4	0.01	0.86	0.021	0.007	0.8	15.74	3.96	0.06	2.74	0.3
E630	0.032	0.54	0.021	0.01	0.37	16.2	4.59	0.68	3.9	0.27

microscope (SEM) were used to observe the microstructure at the cross-sections of the welds.

Results and Discussion

Bead-on-plate welding was first conducted to determine the suitable welding parameters. Figure 4 shows the cross-sections of the weld beads formed by hybrid laser-arc welding. As expected, the weld penetration deepened with a decrease in the welding speed [14, 15]. Based on the obtained weld penetration, a welding speed of 10 mm/s and a Y-groove configuration (see Fig. 3a) were selected in this work. As shown in Fig. 4, there were two issues noted during the hybrid laser-arc welding of 17-4 PH SS: one was related to the porosity and the other one was the centerline cracking at the root of the welds. The cracking susceptibility increased with an increase in the welding speed.

Porosity Mitigation

When the 17-4 PH SS was welded by the arc welding processes (GTAW and SMAW), the porosity was not a large issue, and argon was normally selected as the shielding gas [4–8]. However, severe porosity was observed at the weld beads formed by the hybrid laser-arc welding. The difference between the arc welding and hybrid laser-arc welding was the formation of a keyhole by the high-power laser. The keyhole resulted in the

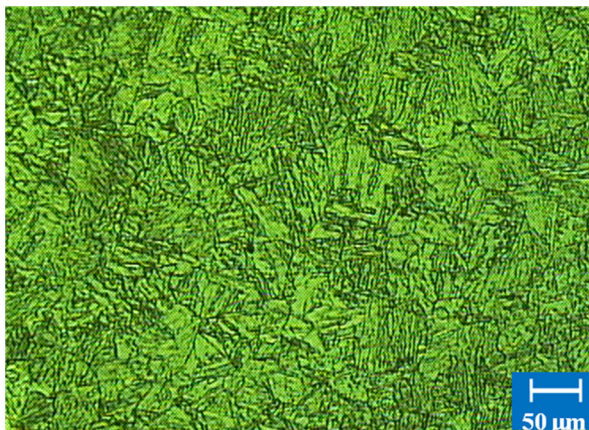


Fig. 1 Microstructure of 17-4 PH stainless steel in an H1150 overaged condition

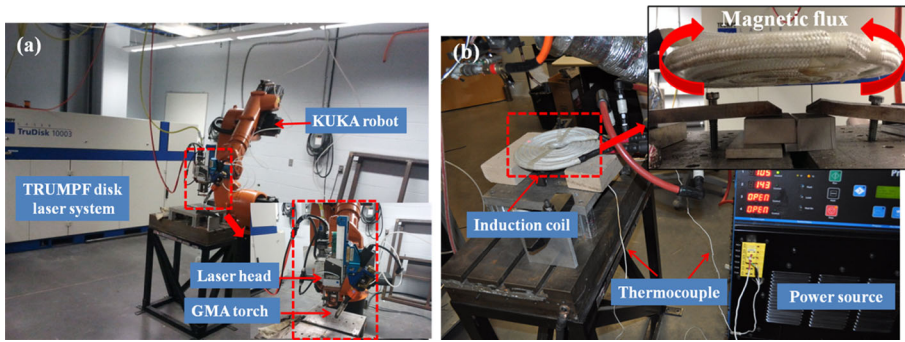


Fig. 2 a Experimental setup; b Induction heater

transformation of the weld bead from being shallow and wide to becoming deep and narrow. The methods to stabilize the keyhole and to prevent the formation of porosity have been investigated by a number of researchers. Kawahito et al. [16] found that a high welding speed could stabilize the keyhole and remove the porosity during the laser welding of AISI 304 stainless steel. Katayama et al. [17] used the hybrid laser-arc welding of austenitic stainless steel and found that a high arc current was helpful to reduce the pores. The keyhole inlet and molten pool were broadened at a high arc current, making it easy for the bubbles generated during welding to escape.

The effects of welding speed and arc current on the porosity during hybrid laser-arc welding of 17-4 PH SS were investigated by performing the bead-on-plate welding. As shown in Fig. 5, the increased welding speed effectively reduced the number of pores in the welds. The porosity almost disappeared at a welding speed of 30 mm/s. Figure 6 shows the longitudinal views of the welds obtained at various arc currents. As shown, the formation of pores was more sensitive to the welding speed than to the arc current. At a low welding speed, the pores notably became severe under a high arc current. As shown in Figs. 6a and b, the porosity presented in the upper region of the weld bead was removed under a higher arc current, in which case, the molten pool was depressed and broadened [17]. Consequently, the bubbles in the upper region of the molten pool easily escaped, leading to the removal of porosity in the upper region of the weld bead.

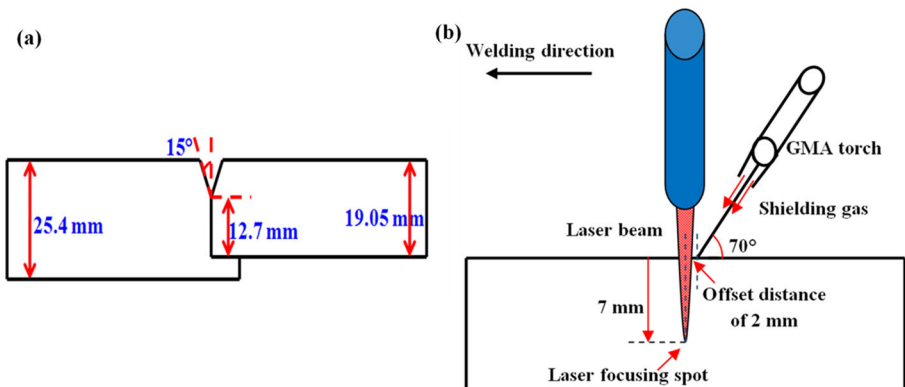


Fig. 3 a Dimensions of the welded coupons; b Position of a laser beam with respect to the GMA torch in the hybrid laser-arc welding process

Table 3 Welding parameters for the hybrid laser-arc welding of 17-4 PH stainless steel

Test no.	Configuration	Laser power, kW	Welding speed, mm/s	Arc current, A	Shielding gas	Shielding gas flow rate, SCFH	Preheating temperature, °C
1	Y-groove	9.9	5	235	Nitrogen	35	–
2	Bead-on-plate	9.9	10	235	Argon	35	–
3	Bead-on-plate	9.9	20	235	Argon	35	–
4	Bead-on-plate	9.9	30	235	Argon	35	–
5	Y-groove	9.9	5	235	Argon	35	–
6	Bead-on-plate	4	10	143	Argon	10	–
7	Bead-on-plate	4	20	143	Argon	10	–
8	Bead-on-plate	4	30	143	Argon	10	–
9	Bead-on-plate	4	10	317	Argon	10	–
10	Bead-on-plate	4	20	317	Argon	10	–
11	Y-groove	4	20	143	Argon	10	–
12	Bead-on-plate	9.9	10	235	Nitrogen	35	–
13	Y-groove	9.9	10	235	Nitrogen	35	200
14	Y-groove	9.9	10	235	Nitrogen	35	300
15	Bead-on-plate	9.9	10	–	Argon	35	–
16	Bead-on-plate	9.9	10	–	Nitrogen	35	–

A high welding speed was effective to mitigate the porosity, but decreased the weld penetration. The full weld penetration was not guaranteed. Thus, this study led to concern for the prevention of porosity at a slow welding speed. Naoki et al. [18] compared the

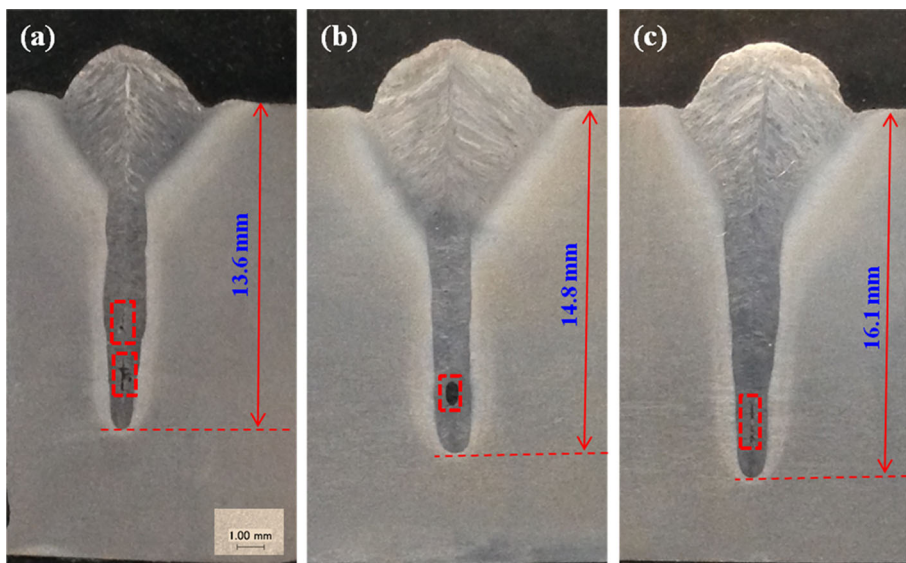


Fig. 4 Cross-sections of the weld beads under various welding speeds: (a) 30 mm/s (Test 4); (b) 20 mm/s (Test 3); and (c) 10 mm/s (Test 2)

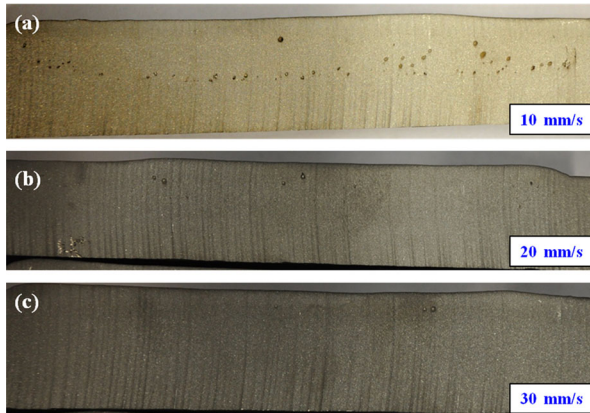


Fig. 5 Effect of the welding speed on the porosity, (a) Test 6, (b) Test 7, and (c) Test 8

effects of helium and nitrogen on the suppression of porosity as the shielding gas during autogenous laser welding of AISI 304 stainless steel. They found that with respect to helium, nitrogen greatly suppressed the porosity formation due to a stable keyhole during welding. Kawahito et al. [19] attributed the stabilization of nitrogen on the keyhole to a high solubility of nitrogen in the molten material. A high content of nitrogen was found in the formed weld. In order to verify the effectiveness of nitrogen on the prevention of porosity in the 17-4 PH SS welds, extreme cases were conducted by using the slow welding speeds of 5 mm/s and 10 mm/s where the keyhole was relatively unstable. As shown in Fig. 7, with respect to the argon, the nitrogen was effective in preventing the formation of porosity even at a very slow welding speed. No pores were observed in the longitudinal views of the welds except at the start of the weld formed with a welding speed of 5 mm/s. Nitrogen as a shielding gas could affect the toughness of the stainless steel weld [20, 21]. However, in this work, the main objective was put on the mitigation of porosity in the weld.

The stability of the keyhole under the shielding gas of argon and nitrogen was investigated by conducting autogenous laser welding at a bead-on-plate configuration. A high-speed charge-coupled device (CCD) camera was used to monitor the dynamics of the plasma. As shown in Figs. 8 and 9, the plasma under different shielding gases showed a similar periodic variation. The keyhole during the laser welding was strongly related to the behavior of plasma above the keyhole inlet. The plasma reflected or absorbed the laser power when the laser passed through. Less laser power reached the substrate when a large plasma occurred above the keyhole inlet, resulting in a decrease in the keyhole size and the plasma. Through a smaller plasma, more laser power hit the base material, leading once again to the growth of keyhole and plasma.

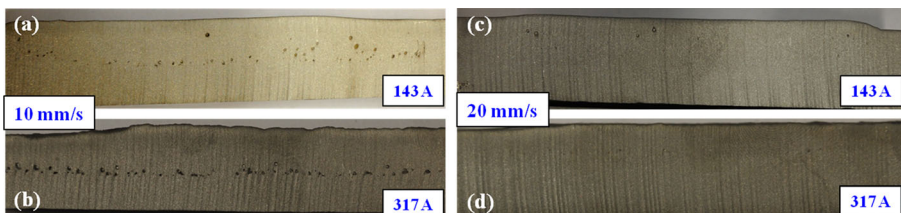


Fig. 6 Effect of the arc current on the porosity, (a) Test 6, (b) Test 9, (c) Test 7, and (d) Test 10

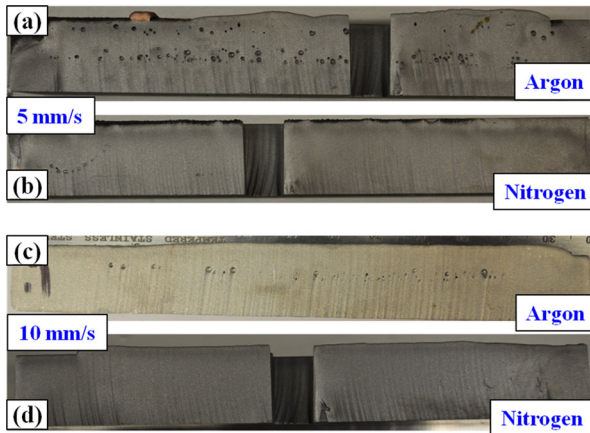


Fig. 7 Effect of the shielding gas on the porosity, (a) Test 1, (b) Test 5, (c) Test 2, and (d) Test 12

However, the plasma intensity was obviously different under the shielding gas of argon with respect to nitrogen. As shown in Fig. 8, the intensity of the plasma was dynamically changed when argon was used as a shielding gas. However, the plasma intensity had little changed under a shielding gas of nitrogen as shown in Fig. 9. This difference was due to the tendency of the shielding gas to form plasma. The shielding gas with a lower molecular weight, higher thermal conductivity, and higher ionization energy generated less plasma [22]. With respect to argon, nitrogen was more effective to suppress the plasma and stabilize the keyhole. The keyhole under nitrogen was more uniform and less fluctuating than when argon was used. A more stable keyhole contributed to the suppression of porosity.

Elimination of Solidification Cracking

Hot cracking was rarely reported during the arc welding of 17-4 PH SS [5]. However, as shown in Fig. 4, the solidification cracking was observed along the weld centerline at the root of the welds obtained in all three cases using hybrid laser-arc welding. In order to investigate the cracking susceptibility of 17-4 PH SS welds, the weld-bead cross-section was studied by an optical microscope and SEM. The welds shown in Fig. 10 were formed by two passes. The first pass was conducted by autogenous laser welding, and the second pass was completed by hybrid laser-arc welding. A large depth/width

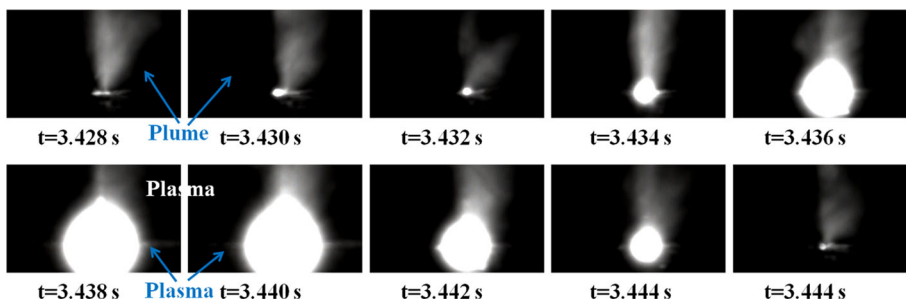


Fig. 8 High-speed CCD camera images about the plasma and plume under the shielding gas of argon (Test 15)

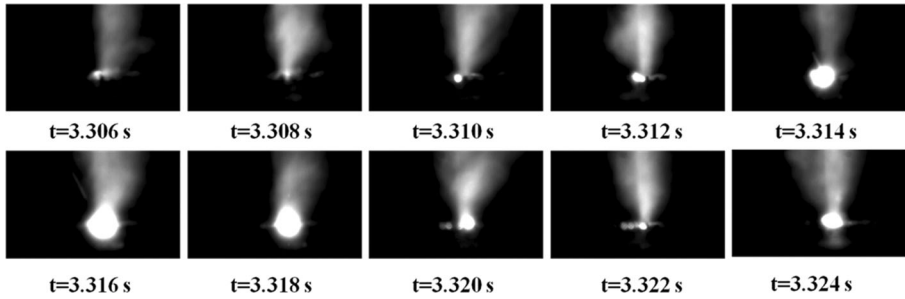


Fig. 9 High-speed CCD camera images of the plasma and plume under the shielding gas of nitrogen (Test 16)

ratio was achieved with both the autogenous laser welding and hybrid laser-arc welding. Centerline cracks were observed in the cross-sections of both welds.

Optical micrographs of the hybrid laser-arc weld along the weld centerline are presented in Fig. 11. The ferrite and martensite were observed at the upper region of the weld. The ferrite and martensite boundaries were distinct. With the weld going deeper, austenite occurred around the region where the solidification cracking formed. The grains became smaller than at the upper region of the weld. Figures 12 and 13 show the SEM images and optical micrographs of the solidification cracking of the welds obtained by hybrid laser-arc welding and autogenous laser welding, respectively. As shown, austenite occurred at the regions surrounding the solidification cracking.

During welding of austenite stainless steel, delta ferrite is beneficial to prevent the solidification cracking. This beneficial effect is related to the solidification sequence. The materials that solidify primarily as austenite are more prone to solidification cracking than the materials that solidify as ferrite [23–25]. In order to investigate the solidification mechanism of 17-4 PH SS during welding, the welding metallurgy of 17-

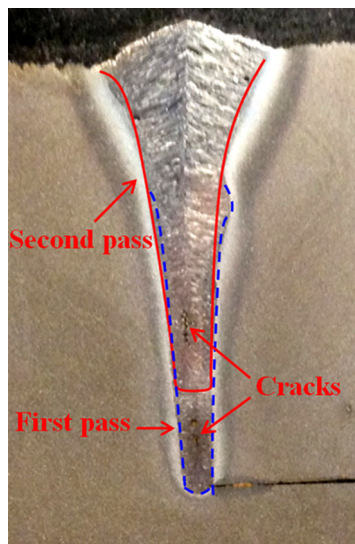


Fig. 10 Cross-sections of the welds formed by autogenous laser welding and hybrid laser-arc welding

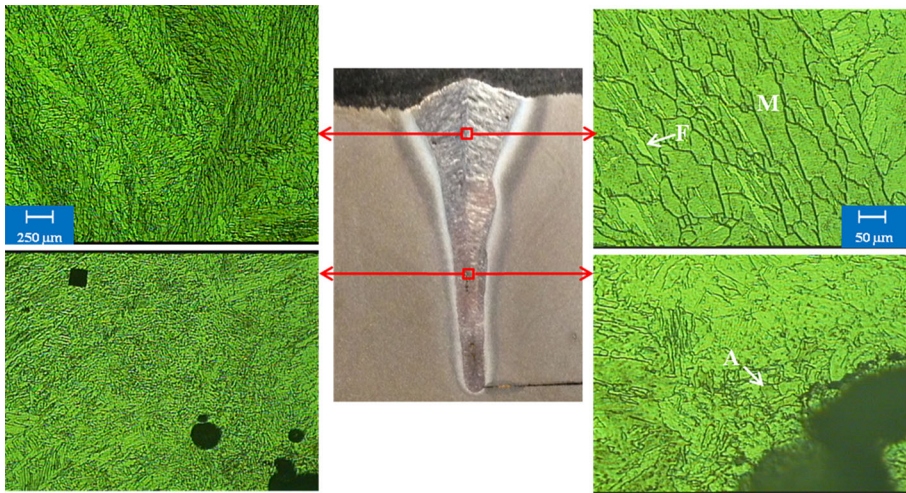


Fig. 11 Optical micrographs of the upper and lower regions of the weld bead. A-austenite, F-ferrite, and M-martensite

4 PH SS was studied. Figure 14 gives the microstructural evolution of 17-4 PH SS during cooling. This appearance sequence of metallurgical phases was achieved through the pseudobinary diagram of the martensitic PH stainless steel in the arc welding processes [5]. As shown, 17-4 PH SS solidifies as a prime ferrite from the liquid state. During cooling, the ferrite largely transforms to austenite due to the solid-

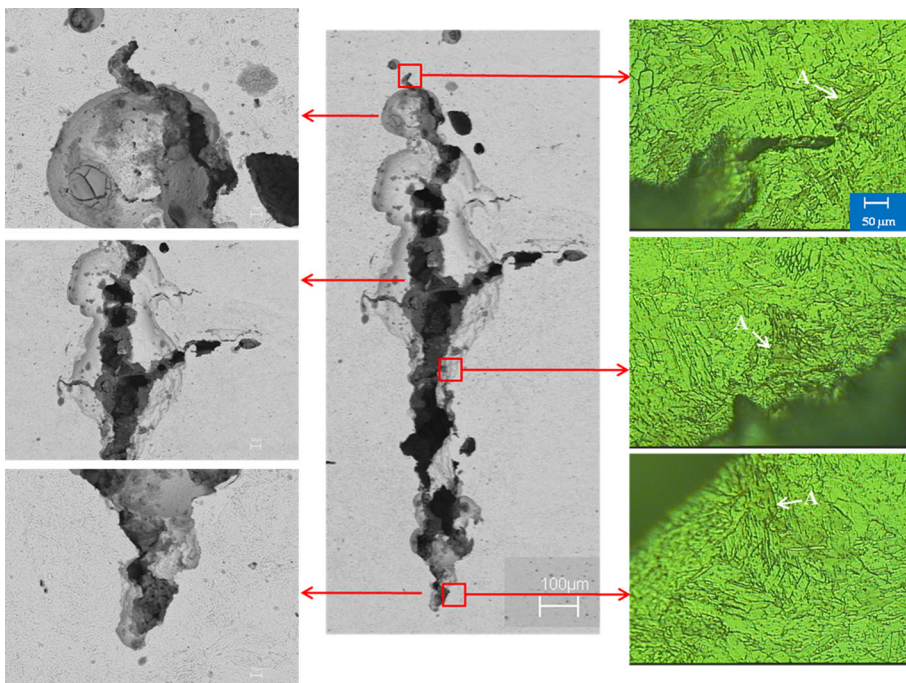


Fig. 12 SEM images and optical micrographs of the centerline cracks in the hybrid laser-arc weld

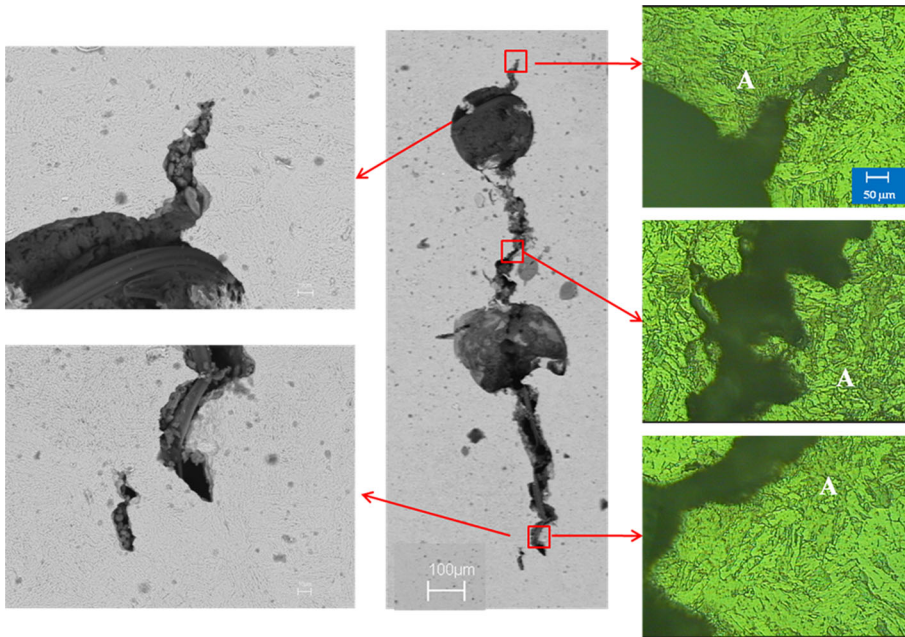


Fig. 13 SEM images and optical micrographs of the centerline cracks in the laser weld

state diffusion [26]. At the martensitic transformation temperature ranging from 132 to 32 °C, austenite fully transforms into martensite. Some residual ferrite is expected in the microstructure of the martensitic PH SS.

Previous scholars predicted the solidification mechanism of the martensitic PH SS by using the ratio of the chromium equivalent to the nickel equivalent (Cr_{eq}/Ni_{eq}). The material compositions were considered as the main factors to determine the solidification behavior. A WRC-1992 diagram [27] provided the equations to calculate Cr_{eq} and

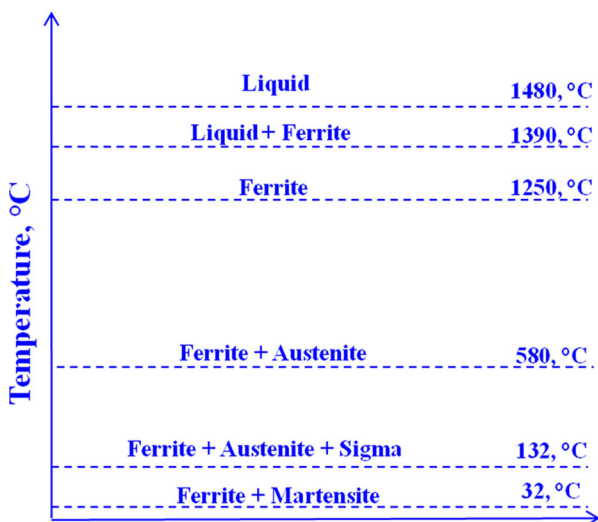


Fig. 14 Appearance sequence of metallurgical phases during cooling for the martensitic PH SS

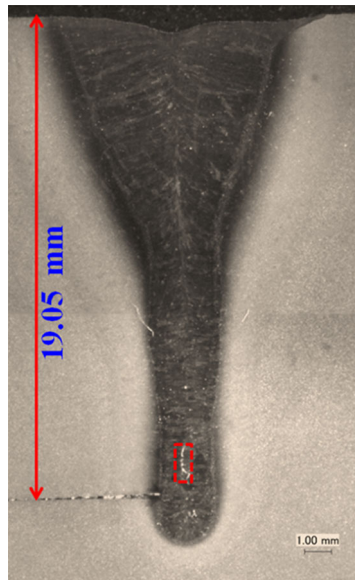


Fig. 15 Cross-section of the weld formed at a preheating temperature of 200 °C (Test 13)

Ni_{ceq} based on the compositions of the materials, where $Cr_{ceq} = Cr + Mo + 0.7Nb$ and $Ni_{ceq} = Ni + 35C + 20N + 0.25Cu$. For 17-4 PH SS and ER630 filler wire, the Cr_{ceq}/Ni_{ceq} ratio is 2.8 and 2.5, respectively. The Cr_{ceq}/Ni_{ceq} ratios are larger than the critical value of 1.5 [4], indicating that the 17-4 PH SS welds solidify as the single ferrite phase. However, under a high cooling rate, the critical Cr_{ceq}/Ni_{ceq} ratio markedly increases [28]. In the case of a high-speed laser welding, using the Cr_{ceq}/Ni_{ceq} method to determine the solidification behavior of 17-4 PH SS is not accurate.

Brooks and Garrison [26] studied the solidification cracking susceptibility of the martensitic PH SS during GTAW. They found that the martensitic PH SS solidified as 100 % ferrite during the arc welding, and the welds showed good resistance to the solidification cracking. However, Brooks et al. [29] pointed out that a rapid cooling rate produced in high-speed laser welding could promote the ferrite to transform into austenite between the liquidus and solidus temperatures. Vitek and David [30] used the laser welding of austenite stainless steel. Their findings noted that the molten material solidified as the single ferrite phase and then transformed to austenite at the solidification stage. The cracking susceptibility increases at the austenitic solidification mode [23–25]. In addition, the grain grows from the opposite sides at the weld center where the impurity elements, such as sulfur and phosphorus, easily segregate due to the enrichment of the free surfaces at the final stage of solidification [31]. This kind of segregation leads to the formation of the low-melting liquid along the grain boundaries. As a result of the tensile stress and strain caused by the restraint of the surrounding structure to the solidification shrinkage, the residual liquid is very prone to fracture. Unfortunately, the high-power laser beam produces a high depth/width ratio, resulting in a higher stress concentration at the root of the weld and a consequent decrease in the cracking resistant of the material [32]. Thus, the narrow region along the weld centerline is suitable to produce the solidification cracking during autogenous laser welding and hybrid laser-arc welding (see Fig. 10).

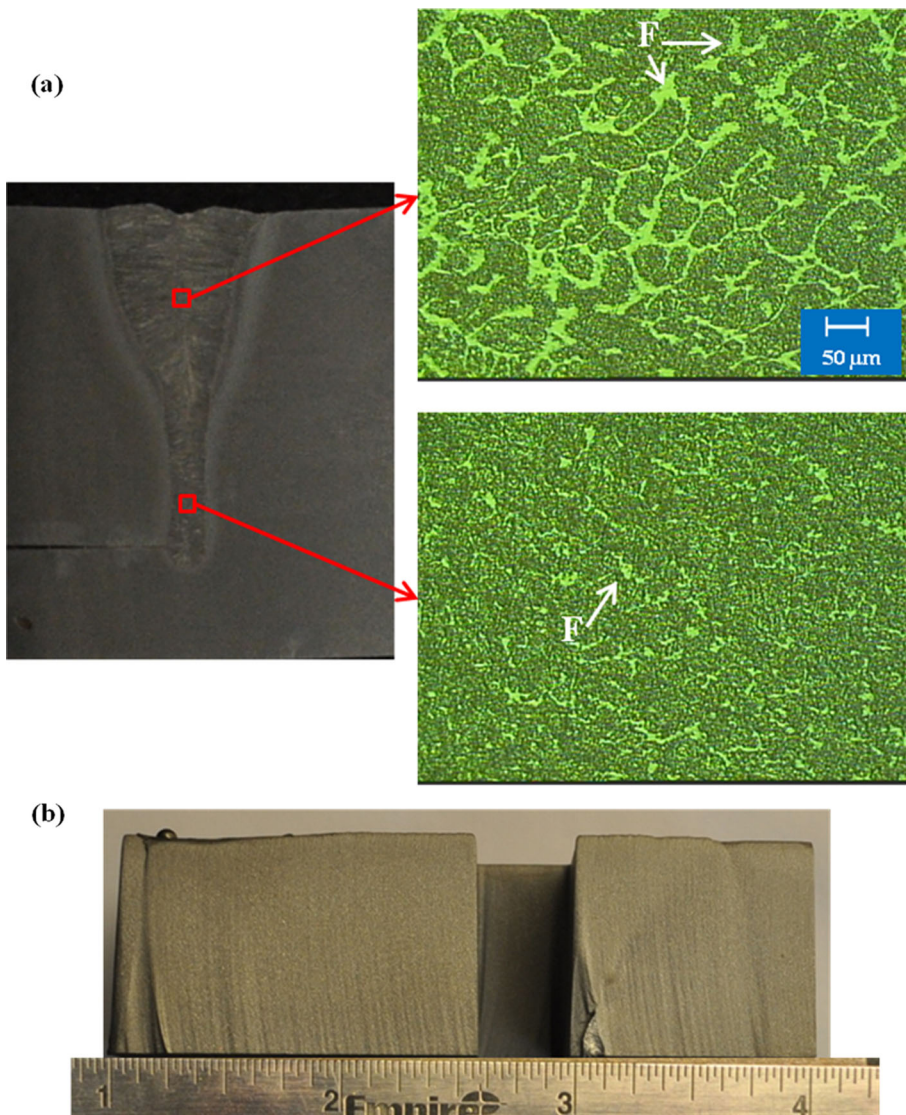


Fig. 16 **a** Cross-section and the optical micrographs of the weld formed at a preheating temperature of 300 °C (Test 14), and **b** the longitudinal view of the weld

During hybrid laser-arc welding, an arc power provided a slow cooling rate in the upper region of the weld. The ferritic solidification mode occurred. Ferrite and martensite were observed in the weld (see Fig. 11). However, the root of the weld was achieved just by the laser power that led to a rapid cooling rate. The austenitic solidification mode appeared. Austenite was observed in the region surrounding the solidification cracking (see Fig. 12). The solidification cracking formed during the hybrid laser-arc welding was induced by two factors: the formation of austenite that was susceptible to cracking, and a large depth/width ratio that caused a high restraint to the solidification shrinkage at the root of the weld. Since the high depth/width ratio was

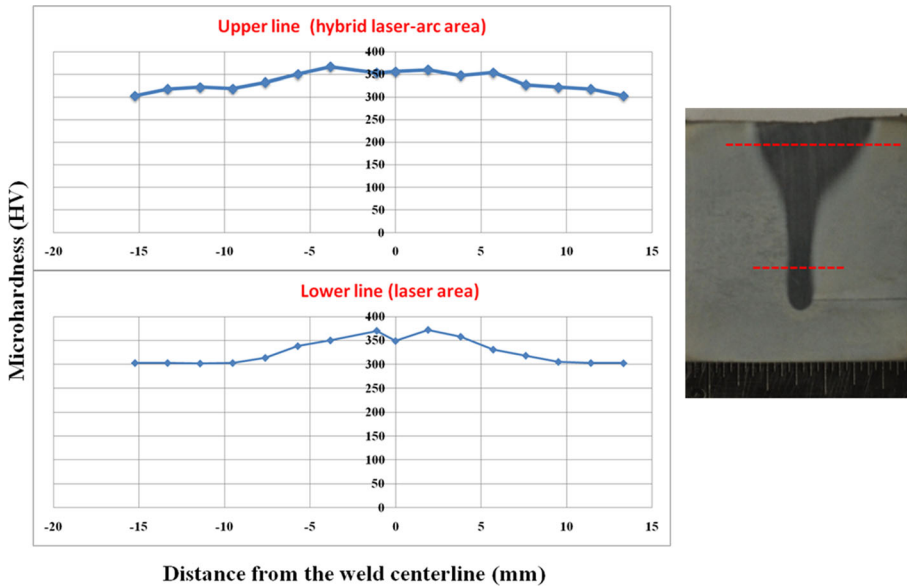


Fig. 17 Microhardness distribution of the weld bead obtained at a preheating temperature of 400 °C

an intrinsic feature of high-power laser welding, the formation of austenite during the solidification stage should be inhibited in order to prevent the solidification cracking in the weld centerline. In this work, the preheating was used to reduce the thermal gradient between the upper region and root of the weld, and to slow the cooling rate at the root of the weld. Figure 15 shows the cross-section of the weld formed at a preheating temperature of 200 °C. It is noted that a 200 °C preheating temperature could not prevent the formation of the solidification cracking. However, the crack size was reduced with respect to the crack shown in Fig. 4c.

In order to completely remove the solidification cracking, the preheating temperature increased to 300 °C. Figure 16a shows the optical micrographs of the obtained weld

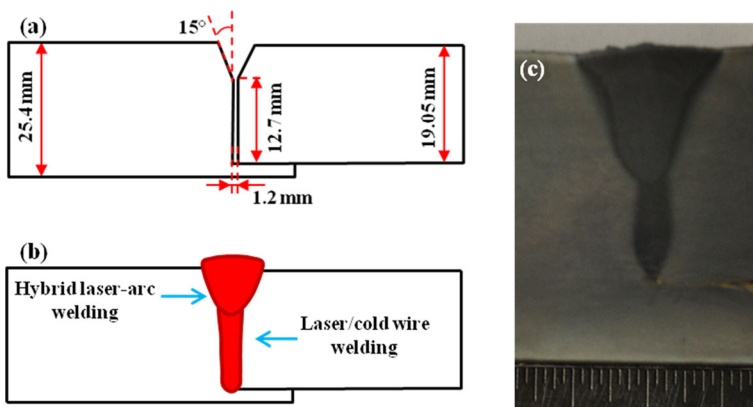


Fig. 18 a Dimensions of the welded sample; b Welding procedures; c Cross-section of the weld bead produced by the two-pass method

Table 4 Welding parameters for the two-pass welding

		Laser power (kW)	Welding speed (mm/s)	Filler wire type	Wire diameter (mm)	Wire feed rate (mm/s)	Current (A)	Preheating (°C)
First pass	Laser/cold wire welding	9	10	ER630	0.9	120	–	300
Second pass	Hybrid laser-arc welding	4	10	ER630	1.2	200	235	None

bead. Ferrite was observed in the upper region and root of the weld, and no cracking occurred. The difference in the ferrite amount indicated that there was still a difference in the solidification conditions between the upper region and root of the weld. But this difference did not lead to the formation of the solidification cracking. As shown in Fig. 16b, no porosity was observed at the longitudinal view of the weld when nitrogen was used as the shielding gas.

Two-Pass Method

The preheating effectively removed the solidification cracks in the weld bead. However, the preheating temperature depended upon the coupon size. For the larger coupons, the minimum preheating temperature to remove the solidification cracks would increase. When the weld length of the coupon shown in Fig. 16 increased to 150 mm, the solidification cracks occurred under the same welding parameters of Test 14. In order to remove the cracking in this long weld length, a preheating temperature of 400 °C was required. Unfortunately, the high preheating temperature would damage the mechanical properties of the weld bead and the base materials. Extra procedures, such as post-weld heat treatment, were required to achieve the desired mechanical properties.

Figure 17 shows the microhardness distribution across the weld bead obtained at a preheating temperature of 400 °C. As shown, there was a relatively uniform hardness plateau across the fusion zone (FZ) of the hybrid laser-arc weld. The hardness in FZ was higher than in the heat affected zone (HAZ) and the base material (BM). The upper region of FZ had a mean hardness value of 350 HV, which was less than the hardness of 370 HV in the lower region of FZ. The higher cooling rate in the lower region of the weld bead led to this higher hardness in FZ. After the preheating, the hardness in BM was 300 HV. However, the achieved BM had a hardness value of around 350 HV. The high preheating temperature attributed to the decrease in the hardness of BM.

In order to lower the preheating temperature, a two-pass method was developed. As shown in Fig. 18b, the first pass was finished by laser welding assisted with a cold wire while a hybrid laser-arc welding was used to fill the groove. During the first pass, the addition of the filler wire decreased the depth/width ratio and relieved the high restraint to the solidification shrinkage at the root of the weld. Consequently, the preheating temperature was reduced from 400 to 300 °C when welding of the coupons with a weld length of 150 mm. As shown in Fig. 18c, the achieved weld bead had no solidification cracks. Table 4 shows the welding parameters used during welding.

Conclusions

Despite 17-4 PH stainless steel having wide applications due to its high yield strength and relatively good corrosion resistance, the weldability of 17-4 PH material is challenging. Conventional welding processes, such as SMAW and GTAW, result in large HAZ and high heat input. The developed hybrid laser welding process has potential to reduce the residual stress from the welding process and retain the properties of the weld metal and HAZ in terms of strength and toughness. The hybrid welding technology will facilitate welding with reduced welding time and heat input to 17-4 PH material in order to retain the material properties. In this study, the 17-4 PH stainless steel plates with a thickness of 19 mm were successfully welded by using hybrid laser welding. The main conclusions are as follows:

- (1) Porosity was easily formed under a shielding gas of argon. A high welding speed effectively reduced the number of pores in the welds. At a lower welding speed, the porosity was prevented by using nitrogen as the shielding gas. Nitrogen had a high solubility in the molten material and stabilized the keyhole, leading to the removal of porosity.
- (2) The 17-4 PH stainless steel was susceptible to the solidification cracking during hybrid laser-arc welding and autogenous laser welding. Two factors led to the solidification cracking: the cracking-susceptible microstructure (austenite) and a high depth/width ratio. At the root of the weld where the solidification cracking occurred, a rapid cooling rate altered the condition of the solidification, the austenitic solidification mode occurred, and ferrite massively transformed into austenite at the final stage of solidification.
- (3) Preheating was used to prevent the formation of the solidification cracks along the weld centerline. The cooling rate and thermal gradient between the upper region and root of the weld were reduced due to the preheating. The transformation of ferrite into austenite during the solidification stage was suppressed. Delta ferrite was observed in the weld bead. The solidification cracking did not occur.

Acknowledgments The financial support by NSF's Grant No. IIP-1034652 is acknowledged. The authors would like to thank the research engineer, Andrew Socha, and Ph.D candidate, Guang Yang, in the Research Center for Advanced Manufacturing, for their help in the execution of experiments.

References

1. AK Steel: PH stainless steel product data bulletin, Middleton, Ohio 17-4 (2000)
2. Bressan, J.D., Daros, D.P., Sokolowski, A., Mesquita, R.A., Barbosa, C.A.: Influence of hardness on the wear resistance of 17-4 PH stainless steel evaluated by the pin-on-disc testing. *J. Mater. Process. Technol.* **205**(1), 353–359 (2008)
3. Tsay, L.W., Yang, T.Y., Young, M.C.: Embrittlement of laser surface-annealed 17-4 PH stainless steel. *Mat. Sci. Eng. A* **311**(1), 64–73 (2001)
4. Das, C.R., Dey, H.C., Srinivasan, G., Albert, S.K., Bhaduri, A.K., Dasgupta, A.: Weldability of 17-4 PH stainless steel in overaged heat treated condition. *Sci. Technol. Weld. Joi.* **11**(5), 502–508 (2006)

5. Lippold, J.C., Kotecki, D.J.: *Welding metallurgy and weldability of stainless steels*, pp. 267–285, Wiley-VCH (2005)
6. Linnert, G.E.: *Welding precipitation-hardening stainless steels*, American Welding Society (1956)
7. Tavakoli Shoushtari, M.R., Moayed, M.H., Davoodi, A.: Post-weld heat treatment influence on galvanic corrosion of GTAW of 17-4 PH stainless steel in 3.5 % NaCl. *Corros. Eng. Sci. Technol.* **46**(4), 415–424 (2011)
8. Nowacki, J.: Weldability of 17-4 PH stainless steel in centrifugal compressor impeller applications. *J. Mater. Process. Technol.* **157**, 578–583 (2004)
9. Bhaduri, A.K., Sujith, S., Srinivasan, G., Gill, T.P.S., Mannan, S.L.: Optimized postweld heat treatment procedures for 17-4 PH stainless steels. *Weld. J.* **74**(5), 153s (1995)
10. Webster, S., Kristensen, J.K., Petring, D.: Joining of thick section steels using hybrid laser welding. *Ironmak. Steelmak.* **35**(7), 496–504 (2008)
11. Jokinen, T., Karhu, M., Kujanpää, V.: Welding of thick austenitic stainless steel using Nd: yttrium–aluminum–garnet laser with filler wire and hybrid process. *J. Laser Appl.* **15**(4), 220–224 (2003)
12. Wu, J.H., Lin, C.K.: Influence of high temperature exposure on the mechanical behavior and microstructure of 17-4 PH stainless steel. *J. Mater. Sci.* **38**(5), 965–971 (2003)
13. Liu, W., Ma, J., Yang, G., Kovacevic, R.: Hybrid laser-arc welding of advanced high-strength steel. *J. Mater. Process. Technol.* **214**(12), 2823–2833 (2014)
14. Gong, X., Lydon, J., Cooper, K., Chou, K.: Beam speed effects on Ti–6Al–4 V microstructures in electron beam additive manufacturing. *J. Mater. Res.* **29**(17), 1951–1959 (2014)
15. Gong, X., Anderson, T., Chou, K.: Review on powder-based electron beam additive manufacturing technology. *Manuf. Rev.* **1**, 1–12 (2014)
16. Kawahito, Y., Mizutani, M., Katayama, S.: Elucidation of high-power fiber laser welding phenomena of stainless steel and effect of factors on weld geometry. *J. Phys. D. Appl. Phys.* **40**(19), 5854 (2007)
17. Katayama, S., Naito, Y., Uchiumi, S., Mizutani, M.: Physical phenomena and porosity prevention mechanism in laser-arc hybrid welding. *Trans. JWRI* **35**(1), 13 (2006)
18. Seto, N., Katayama, S., Matsunawa, A.: High-speed simultaneous observation of plasma and keyhole behavior during high power CO₂ laser welding: effect of shielding gas on porosity formation. *J. Laser Appl.* **12**(6), 245–250 (2000)
19. Kawahito, Y., Mizutani, M., Katayama, S.: High quality welding of stainless steel with 10 kW high power fiber laser. *Sci. Technol. Weld. Joi.* **14**(4), 288–294 (2009)
20. Szumachowski, E.R., Reid, H.F.: Cryogenic toughness of SMA austenitic stainless steel weld metals: part II—role of nitrogen. *Weld. J.* **58**(2), 34–44 (1979)
21. Whipple, T.A., McHenry, H.I., Read, D.T.: Fracture behavior of ferrite-free stainless steel welds in liquid helium. *Weld. J.* **60**(4), 2117 (1981)
22. Reisgen, U., Schleser, M., Mokrov, O., Ahmed, E.: Shielding gas influences on laser weldability of tailored blanks of advanced automotive steels. *Appl. Surf. Sci.* **257**(5), 1401–1406 (2010)
23. Hull, F.C.: Delta Ferrite and Martensite formation in stainless steels. *Weld. J.* **52**(5), 193 (1973)
24. Lippold, J.C.: Centerline cracking in deep penetration electron beam welds in Type 304 L stainless steel. *Weld. J.* **64**(5), 127s–136s (1985)
25. Kujanpää, V., Suutala, N., Takalo, T., Moisoio, T.: Correlation between solidification cracking and microstructure in austenitic and austenitic-ferritic stainless steel welds. *Weld. Res. Int.* **9**(2), 55–77 (1979)
26. Brooks, J.A., Garrison, W.M.: Weld microstructure development and properties of precipitation-strengthened martensitic stainless steels. *Weld. J.* **78**, 280-s (1999)
27. Kotecki, D.J., Siewert, T.A.: WRC-1992 constitution diagram for stainless steel weld metals: a modification of the WRC-1988 diagram. *Weld. J.* **71**(5), 171–178 (1992)
28. Kou, S.: Solidification and liquation cracking issues in welding. *JOM* **55**(6), 37–42 (2003)
29. Brooks, J.A., Baskes, M.I., Greulich, F.A.: Solidification modeling and solid-state transformations in high-energy density stainless steel welds. *Metal. Trans. A* **22**(4), 915–926 (1991)
30. Vitek, J.M., Dasgupta, A., David, S.A.: Microstructural modification of austenitic stainless steels by rapid solidification. *Metal. Trans. A* **14**(9), 1833–1841 (1983)
31. Kadoi, K., Fujinaga, A., Yamamoto, M., Shinozaki, K.: The effect of welding conditions on solidification cracking susceptibility of type 310S stainless steel during laser welding using an in-situ observation technique. *Weld. World* **57**(3), 383–390 (2013)
32. Shankar, V., Gill, T.P.S., Mannan, S.L., Sundaresan, S.: Solidification cracking in austenitic stainless steel welds. *Sadhana* **28**(3–4), 359–382 (2003)